HHS Public Access

Author manuscript

J Biomech. Author manuscript; available in PMC 2018 January 04.

Published in final edited form as:

J Biomech. 2017 January 04; 50: 180–187. doi:10.1016/j.jbiomech.2016.11.041.

The Manifestation of Vortical and Secondary Flow in the Cerebral Venous Outflow Tract: An In Vivo MR Velocimetry Study

Sarah Kefayati[†], **Matthew Amans**[†], **Farshid Faraji**[†], **Megan Ballweber**[†], **Evan Kao**[†], **Sinyeob Ahn**[‡], **Karl Meisel**[*], **Van Halbach**[†], and **David Saloner**[†,§]

[†]Department of Radiology and Biomedical Imaging, UCSF, San Francisco, CA, USA

[*]Department of Neurology, UCSF, San Francisco, CA, USA

[‡]Siemens Healthcare, CA, USA

[§]Radiology Service, VA Medical Center, San Francisco, USA

Abstract

Aberrations in flow in the cerebral venous outflow tract (CVOT) have been implicated as the cause of several pathologic conditions including idiopathic intracranial hypertension (IIH), multiple sclerosis (MS), and pulsatile tinnitus (PT). The advent of 4D Flow magnetic resonance imaging (4D-Flow MRI) has recently allowed researchers to evaluate blood flow patterns in the arterial structures with great success. We utilized similar imaging techniques and found several distinct flow characteristics in the CVOT of subjects with and without lumenal irregularities. We present the flow patterns of 8 out of 38 subjects who have varying heights of the internal jugular bulb and varying lumenal irregularities including stenosis and diverticulum. In the internal jugular vein (IJV) with an elevated jugular bulb (JB), 4DFlow MRI revealed a characteristic spiral flow that was dependent on the level of JB elevation. Vortical flow was also observed in the diverticula of the venous sinuses and IJV. The diversity of flow complexity in the CVOT illustrates the potential importance of hemodynamic investigations in elucidating venous pathologies.

Keywords

Cerebral venous flow; 4D-Flow MRI; pulsatile tinnitus; jugular vein; vortical flow

I. INTRODUCTION

Aberrations in the cerebral venous outflow tract (CVOT) have been implicated as the cause of several pathological conditions including multiple sclerosis (MS) (Khan et al., 2010;

Corresponding author (Sarah Kefayati) at: Department of Radiology and Biomedical Imaging, University of California San Francisco, Room BA32, VA Medical Center, 4150 Clement Street, San Francisco, CA, USA, 94121. Tel.: + 1 415 221 4810 x 23802.

Conflict of Interest

There is no conflict of interest to be declared.

Weir, 2010), pulsatile tinnitus (PT) (Dietz et al., 1994; Krishnan et al., 2006; Mehall et al., 1995; Weissman and Hirsch, 2000), and idiopathic intracranial hypertension (IIH) (Satti et al., 2015; Starke et al., 2015). MS association with internal jugular vein (IJV) stenosis has been quite controversial with some groups suggesting association (McTaggart et al., 2012; Zamboni et al., 2009), and others refuting the association (Sundstrom et al., 2010; Wattjes et al., 2011). Several venous etiologies for PT have been suggested including high-riding jugular bulb, venous sinus stenosis, sinus and jugular vein diverticulum and venous webs (Amans et al., 2014; Chiarella et al., 2012; Hofmann et al., 2013; Krishnan et al., 2006; Madani and Connor, 2009). Several open and endovascular interventions have even been developed to treat anomalies of the CVOT (Ahmed et al., 2011; Eisenman, 2011; Houdart et al., 2000; Starke et al., 2015). However, anatomic variance is quite wide and lumenal irregularities such as sinus stenosis may not always be pathologic (Durst et al., 2016). Figure 1 shows the structure of the CVOT anatomy within the head.

Despite a surge of clinical interest in cerebral venous pathology, the hemodynamics of CVOT remains largely unexplored. Previous venous flow studies, the majority of which are related to investigations of venous insufficiency as a potential cause of MS, have focused on stroke volume flow and flow pulsatility factors using 2D measurements performed with extracranial Doppler ultrasound, (Baracchini et al., 2011; Zamboni et al., 2009), and more recently with advanced magnetic resonance imaging (MRI) methods (Feng et al., 2012; Wattjes et al., 2011).

MRI has emerged as a comprehensive imaging modality capable of providing detailed anatomic (via MR angiography) and hemodynamic imaging. Flow rate and waveform are provided by 2D flow measurements. Volumetric velocity fields can be measured across the cardiac cycle enabled by 4DFlow phase-contract MRI (PC-MRI).

4DFlow MRI has been used to study hemodynamics of a variety of arterial structures, ranging literally and figuratively from head to foot (Dyverfeldt et al., 2015; Markl et al., 2014; Pereira et al., 2016; Roldan-Alzate et al., 2016). Volumetric 3-component velocity-encoded measurements enable a variety of velocity-field-based analyses including streamline visualization, wall shear stress, 3D pressure difference maps, as well as turbulence-induced parameters such as turbulent kinetic energy (TKE), and energy losses. It is also important to acknowledge the major challenges of 4Dflow MRI most of which constitute active research areas: these include limitations due to spatial and temporal resolution, noise and systemic errors, and inability to resolve instantaneous and small-scale velocities.

The wide range of outcomes in studies evaluating the effects of the CVOT on patient health suggests the CVOT to be complex and that many factors relevant to this vascular structure, including the volumetric velocity field, remain unknown. As a step in determining the effects of the CVOT to patient health, we sought to analyze the volumetric velocity field characteristics of the CVOT. This observational study presents the potential of advanced MR flow imaging identifying different categories of flow behavior in the variable geometries of the CVOT. In pursuit of this aim, we performed *in vivo* MRI studies on subjects with a range of representative CVOT geometries and lumenal irregularities to determine the extent to

which lumenal boundary conditions dictate the dominant flow patterns and induce secondary flow features. The subjects either had CVOT-associated symptoms or were asymptomatic.

II. METHODS

A. *In Vivo* MR Imaging

A series of MRI protocols, approved by our institution's Institutional Review Board (IRB), were implemented to evaluate the anatomy and flow in the jugular vein outflow tract. All imaging was performed on a Siemens 3T Skyra scanner, (Siemens Medical Systems, Erlangen, Germany). A 3D MR venogram was obtained using a contrast-enhanced MR angiogram (CE-MRA) acquired in the venous phase and administration of intravenous Gadolinium-DTPA (Gd-DTPA). First, a series of low-resolution CE-MRA images were acquired at one-second intervals to determine the arrival time of contrast in the jugular vein. For the bolus timing run, acquisition was initiated simultaneously with injection of 2cc Gd-DTPA delivered at 2cc/sec followed by a 15cc saline flush at 2cc/sec. The best estimate of the arrival time of the contrast to the jugular vein from the injection time, T_{delay}, was determined by visually inspecting the resulting maximum intensity projection (MIP) of the acquired images. A 3D CE-MRA with isotropic resolution of 0.7-mm was then acquired beginning at T_{delay} after injection of the full contrast bolus of 20cc Gd followed by a 15cc saline flush, all injected at 2cc/sec and took about 34 s. The volumetric imaging slab covered the entire dural venous sinuses including the superior sagittal sinus, paired transverse sinuses (TS), sigmoid sinuses (SS), and internal jugular veins (IJV) with full extension along the neck. The imaging volume had an in-plane matrix of 240×320, FOV=167×223 mm^2, slice thickness of 0.7 mm, and 144 slices.

2D flow data sets were acquired using a cardiac-gated 2D PC-MRI sequence in 3 planes: through the left sigmoid sinus, through the right sigmoid sinus, and through the distal IJV capturing both left and right sides. A representative set of imaged vessel diameters (D) for 2D flow rate measurements from the right (RT) and left (LT) side of the SS and IJV are $D_{ss\text{-}RT}$ = 8.5 mm, $D_{ss\text{-}LT}$ = 3 mm, $D_{IJV\text{-}RT}$ = 6.7 mm, $D_{IJV\text{-}LT}$ = 3.8 mm. The acquisition time was ~ 25 s for each set. Other typical imaging parameters include imaging matrix = 192×256, in-plane resolution = 0.78×0.78 mm^2, FOV=150×200, slice thickness = 5 mm, covered phase window >800 ms, and velocity encoding (VENC) = 100 cm/s

4D MR velocimetry was performed using phase-contrast (PC) MRI. The prospectively gated study had an acquisition time of about 10 minutes. Data was reconstructed in phases at 80 ms intervals providing 9–12 phases depending on subject-specific heart rate. The volumes of interest were selected by assessing the MIPs from the CE-MRA and were based on the geometry, caliber, and location of the abnormalities. Also, prior to 4D flow imaging, the VENC value was optimized to assure proper dynamic range coverage of velocities and avoid phase-wrapping artifacts that can occur if this value is set too low. For the CVOT, asymmetry in side dominancy and the presence of pronounced stenosis influences the setting of the VENC value. To find the optimum VENC, 2D-flow imaging was applied in the narrowest part of CVOT included in the FOV. Starting from a VENC of 75 cm/s, this measurement was repeated until the lowest optimal VENC value was achieved by assessing the phase image for possible aliasing. For the group of presented subjects the selected

VENC was either 100 or 150 cm/s and set to the same value for all three encoding directions. Other setting parameters include: flip angle = 8°, isotropic resolution = $1.3\times1.3\times1.3$ mm^3, a typical in-plane imaging matrix = 116×176, FOV = 151×230 mm^2, Number of slices = 24–28, echo:repetition time = 4:8 s, acceleration factor = 3.

B. Selected Subjects

The anatomies from the eight subjects were selected for purposes of illustration of variance from the 38 subjects enrolled in our ongoing work in evaluating patients suspected of venous pathology and control subjects. All patients signed written informed consent to participate in this study.

The anatomies from all the subjects were divided in terms of whether the surface of the vessels in the CVOT had any focal changes in surface smoothness. They were thus classified as either having a smooth surface or an irregular surface. The irregular surface group includes subjects with identifiable lumenal irregularities such as diverticula (i.e. lobular lumenal protrusions) or outpouchings, sinus stenoses, or arachnoid granulations (i.e. filling defect). The smooth surface group excludes any lumenal abnormalities and includes anatomies with varying levels of elevation of the jugular bulb (JB) above the level of the sigmoid sinus junction. Moderately tapering stenoses of the IJV were considered within the smooth surface scope as they are frequently reported in both healthy and patient populations (Jayaraman et al., 2012). Six IJVs from five subjects (from the total of eight) are included in the smooth surface group and five CVOT from five subjects (from the total of eight) are included in the irregular surface group. There is overlap of two of the subjects in both groups resulting in a total of eight subjects.

C. Image Post-processing

Using in-house Python code based on the PyQt, VTK, and VMTK packages, the DICOM images were post-processed. A mask was extracted from the so-called speed images, which is the modulus of the phase shift along each of the three encoding axes. This was performed on the peak systolic image and thresholding was performed on those images with the boundary set for the zero-velocity value. One of the necessary post-processing steps is correction of background phase offsets - introduced by sources such as magnetic field inhomogeneity and eddy currents – that unlike some of the correction terms, including Maxwell correction and gradient non-linearity correction, is not accounted for in the online image reconstruction on the scanner platform. In our pipeline, the background correction is performed by fitting a polynomial function through the surrounding stationary tissue (Dyverfeldt et al., 2015). Streamline visualization was performed during the post-processing to monitor any undesired effect such as non-physiological incident of streamlines on the vessel wall at an acute angle. The background correction was adjusted iteratively to minimize the presentation of this effect. Next, an advanced denoising filter developed by Ong et al. (Ong et al., 2015) was applied to the background corrected velocities. This denoising technique is based on the divergence-free property of incompressible flow and accounts for non-divergence-free flow components while retaining the meaningful flow features.

The residual effect of MR imaging imperfection moderately affects the conservation of mass. To depict the level of mass conversation of our 4D velocity fields after the post-processing steps, flow rates derived from 4D PC-MR images were estimated in the reference geometry in two segments: with and without auxiliary branches. As shown in Figure 2, in the part where there is no connecting vessel (in the sigmoid sinus) smaller flows rate variation (max. SD = 0.54 ml/s, min. SD = 0.30 ml/s) are present as compared to the downstream IJV (max. SD = 1.20 ml/s, min. SD = 0.36 ml/s).

ParaView (Ayachit, 2015) and Osirix were used to create streamline visualizations and MIPs from CE-MRA, respectively.

For vessels with a smooth surface, the helicity index (*HI*) was employed to demonstrate and quantify the helical quality of the flow in the IJV (Grigioni et al., 2005). *HI* is defined as a unitless normalized entity based on the angle between the velocity and its corresponding vorticity vector $(HI=\frac{V.(\nabla \times V)}{|V||\nabla \times V|})$ which yields −1<*HI*<1. *HI* magnitude is one for purely helical flow. This value is zero for purely axial flow. By definition, *HI* is also zero if the vortex lies in a plane, i.e. purely rotational flow. The presented HI is for one time-point and the HI_{mean} is obtained by averaging over space with the spatial extent defined superiorly by the apex of the jugular bulb and inferiorly by the level of the C1-transvere process. To more intuitively convey the tightness and the spatial pitch of the spiral flow, we define the singular quantity of helicity pitch -*HP*- as the inverse value of $HI_{\mathrm{mean}}(HP=\frac{1}{HI_{\mathrm{mean}}})$.

III. RESULTS

A. 2D-Flow Characteristics

2D flow analysis (i.e. flow rate vs. time) of the CVOT provides information on flow pulsatility and the distribution of total blood flow, and hence information on dominant and non-dominant outflow tracts.

Figure 3 shows three examples of 2D flow characteristics measured at two locations of the CVOT, SS and downstream IJV, both for the left and right side. Table 1 provides a summary of the plots in form of mean flow and pulsatility index. Assessing several 2D flow patterns from various subjects, the following general observations can be made which are represented with these three examples: first, there is substantial inter-individual differences in the pulsatility index but it is higher in the IJV flow as compared to in the SS. Secondly, the flow distribution between the dominant and non-dominant side can vary significantly from individual to individual. Third, flow rate can either increase or decrease over the cardiac cycle at the IJV compared to the SS depending on flow contributions in other draining or supplying vessels at the junction of the SS and the IJV.

B. Smooth Surface Group

Figure 4 shows the anterior view of the anatomies of a group of smooth surface IJVs. The JB elevation from the level of the sigmoid sinus junction varies increasing from left to right. The left and right IJVs in the same individual can have distinctly different anatomies.

The velocity streamline visualizations at peak systole for the anatomies presented in Figure 4 are shown in Figure 5 in both anterior (top panel) and lateral (bottom panel) views. The core flow is more impacted by the elevation of the JB than the peripheral flow patterns are. As such, to highlight the effect of the height of the JB relative to the SS insertion, the core flow is shown in denser and more intense streamlines. Flow evolution over the cardiac cycle can be seen in the supplementary-video 1 depicting the path-line visualization for Subject E-RT.

With increase in the level of bulb elevation, a more pronounced spiral flow pattern emerges in the core flow manifested by tighter vortical rings, and thus greater *HP* values as shown in Figure 6 for four of the smooth surface geometries depicted in Figure 4. The spiral pattern extends caudally to the level of the C1-transvere process. The jugular vein is often compressed across the C1 transverse process, which may limit the transmission of the spiral pattern. The stenosis of the IJV at the C1 transverse process is also recognizable by the higher velocity jet downstream (caudally) from the stenosis in IJVs seen in Figure 5 resulting in peak velocities of 0.85 m/s and 0.5 m/s for Subject E-RT and Subject C-LT respectively.

C. Irregular Surface Group

As defined earlier, the irregular surface group includes CVOT geometries with lumenal anomalies such as stenoses or outpouchings. Figure 7 shows five representative irregular surface geometries. Three of the anatomies exhibit irregularities of JB and the other two demonstrate irregularities of the transverse and sigmoid sinuses. Subject B-LT depicts a diverticulum of the JB seen as a focal polypoid extension superiorly. Subject F-RT illustrates an anatomy with two diverticula, one located medially and one laterally and posterior to the JB. Subject C-RT shows an anatomy with an outpunching posterior to the JB at the junction with condylar vein confluence. The anatomy depicted in Subject G-RT contains three abnormal features including a TS stenosis, sigmoid sinus diverticulum, and a sigmoid sinus filling defect on the MIP presumed to be an arachnoid granulation. Subject H-RT shows the CVOT anatomy with a severe TS stenosis upstream of a laterally projecting sigmoid sinus diverticulum.

Figure 8 shows the peak systole flow pattern for the matching geometries and orientations presented in Figure 7. The two jugular diverticula seen in Subject F-RT result in two separate vortical flow regions merging into the spiral flow of the IJV that is induced by the elevated bulb. Flow evolution created by the path-line visualization over the cardiac cycle for Subject F-RT can be seen in the supplementary-video 2.

The filling defect abnormality seen in Subject G-RT results in formation of two high-velocity jets – with a peak velocity of 0.9 m/s – in the sigmoid sinus downstream of the diverticulum. The upstream jet flow originated in the transverse sinus extends to the diverticulum located directly downstream of the stenosis. Despite the large size, the flat shape of the diverticulum results in a planar vortex flow, as opposed to a spiral flow seen for the diverticula with a more saccular shape such as shown for Subject H-RT. The vortical flow pattern is also observed in Subject C-RT for the with an out-pouching posterior to the

JB. The medial side of the out-pouching connects to the anterior condylar vein confluence as seen in Figure 7- Subject C-RT.

Apart from the sinuses, flow in the IJV exhibits similar patterns to those in the smooth surface group mediated mainly by the geometry of the jugular bulb. Supplementary Figure 1 shows the helical flow for the irregular surface group with elevated jugular bulb.

IV. DISCUSSION

In our limited series, we have illustrated several distinct flow characteristics in the CVOT in subjects with and without lumenal irregularities. In subjects without lumenal irregularity, the spiral/vortical flow characteristic in the internal jugular vein is induced by the extent to which the jugular bulb rises above the level of the sigmoid sinus junction. Due to its volumetric nature, this flow property will not be fully appreciated on cross-sectional 2D flow mappings (Wattjes et al., 2011; Zamboni et al., 2009). In our experience, 4D flow phase image with anterior-posterior encoding direction in the coronal orientation of the IJV with an elevated bulb appears as two distinct adjacent bright and dark areas. This unique feature indicates flow in two opposing directions (in and out of plane) and reflects the rotational property of the flow along the vertical axis of the IJV. For the same slice orientation but for phase images with head-foot (superior-interior) encoding, the flow region in the IJV appears with similar brightness indicating that flow is in the same direction. This underscores the importance of multi-directional flow imaging in determining flow dynamics and secondary flows.

The superior extent of the JB is highly variable in smooth surface subjects and this may be in part due to its development. The JB is not present at birth, but is an anatomical development resulting from the hemodynamic forces of the negative pulse waves ascending from the right atrium (Okudera et al., 1994). A high or high-riding JB is characterized by a JB that rises to the floor level of certain parts of the auditory system such as in proximity to the middle ear (Weissman and Hirsch, 2000). Angiographers have long noted great variety in the height of the jugular bulb, yet high JB can sometimes cause a debilitating symptom such as pulsatile tinnitus (Sonmez et al., 2007; Waldvogel et al., 1998). One of the main observational hemodynamic findings presented in this study is the varying spiral/vortical flow quality that is manifested as different tightness of curl in flow patterns as was shown across a series of geometries with varying jugular bulb elevations. Investigations of how possible morphological changes of the JB lumen would modify flow patterns in the IJV are a subject of future investigation. It would also be of interest to study the interplay of IJV flow and JB wall motion to explore the potential impact of that on erosion of the surrounding bony structure.

Flow patterns induced by CVOT irregularities such as stenosis resemble stenoses evaluated in the arterial system such as a jet of flow and downstream recirculation (Kefayati et al., 2014). Subjects with diverticula seem to have recirculation within the diverticula similar to the recirculation effects seen in intracranial aneurysms (Rayz et al., 2008). For the presented geometries, it is also interesting to note the presence of the TS diverticula in the direct path of the jet flow induced by an upstream stenosis. This observation, which has been reported

previously (Gard et al., 2009), indicates a potential role of an upstream stenosis in remodeling effects and formation of a downstream diverticulum.

Reports of pulsatile tinnitus resolution, either by stent placement in the transverse/sigmoid sinus stenosis (Signorelli et al., 2012), or by coil embolization of the diverticulum located downstream of a stenosis (Amans et al., 2014), is suggestive that the blood flow patterns demonstrated by this study may be causative of pulsatile tinnitus.

There is a great degree of variance in the cerebral venous system. A recent analysis of 355 computed tomography angiography with venous phase timing obtained in subjects without a potentially venous medical problem demonstrated an 18% prevalence of unilateral asymptomatic venous sinus stenosis and 16% prevalence of unilateral venous hypoplasia (Durst et al., 2016). However, sinus stenosis has been recently implicated as either a cause or effect of IIH, and treatment of the stenosis can treat IIH (Satti et al., 2015). It is likely that flow patterns in the sinus may differ between benign and pathologic stenoses if the latter are accompanied by turbulent flow. We are optimistic that the future use of advanced 4D flow methods may provide the link that will allow us to differentiate between those two conditions.

2D-flow analysis of CVOT can offer valuable insights into the presenting pathology such as information on a distinctly lower pulsatility index in the sigmoid sinus compared to the IJV, as reported in this study and the potential impact that this might have on regulating the intracranial pressure requires further exploration (Stoquart-ElSankari et al., 2009). Nevertheless, only time-resolved volumetric flow measurements, such as those clinically offered by 4D-Flow MRI, can provide the necessary information for analysis of hemodynamic induced phenomena such as cerebral venous vasculature remodeling, morphological changes, flow regulation, lumenal wall motion, TKE analysis (Kefayati et al., 2016), and bruit generation with venous etiology and this defines the scope of our future studies.

V. CONCLUSION

The wide range of anatomic variance and abnormalities present in the cerebral venous tract induce a wide spectrum of flow complexity. Specifics of presenting flow requires an analysis of the velocity field through the full 3D space, such as is provided 4D-flow MR imaging. Vortical flow is the principle secondary flow pattern emerging in this vascular territory due to unique geometrical features such as elevated jugular bulbs or diverticula. Stenosis/narrowing is another abnormally or anatomically occurring feature of this vascular structure that can result in downstream flow disturbances. The implications of these hemodynamic features in the various pathologies of cerebral venous tract require further investigation.

Supplementary Material

Refer to Web version on PubMed Central for supplementary material.

Acknowledgments

The authors would like to acknowledge Dr. Wade Smith for his helpful discussions that helped to prompt the authors to undertake this work. The authors would also like to thank all the participants for their enthusiasm. Financial support is acknowledged from the National Institutes of Health (HL114118 (DS), NS059944 (DS)).

References

Ahmed RM, Wilkinson M, Parker GD, Thurtell MJ, Macdonald J, McCluskey PJ, Allan R, Dunne V, Hanlon M, Owler BK, Halmagyi GM. Transverse sinus stenting for idiopathic intracranial hypertension: A review of 52 patients and of model predictions. American Journal of Neuroradiology. 2011; 32:1408–1414. [PubMed: 21799038]

Amans MR, Stout C, Dowd CF, Higashida RT, Hetts SW, Cooke DL, Narvid J, Halbach VV. Resolution of pulsatile tinnitus after coil embolization of sigmoid sinus diverticulum. Austin Journal of Cerebrovascular Disease & Stroke. 2014; 1

Ayachit, U. The paraview guide: A parallel visualization application. Kitware, Incorporated; 2015.

Baracchini C, Perini P, Calabrese M, Causin F, Rinaldi F, Gallo P. No evidence of chronic cerebrospinal venous insufficiency at multiple sclerosis onset. Annals of Neurology. 2011; 69:90–99. [PubMed: 21280079]

Chiarella G, Bono F, Cassandro C, Lopolito M, Quattrone A, Cassandro E. Bilateral transverse sinus stenosis in patients with tinnitus. Acta Otorhinolaryngologica Italica. 2012; 32:238–243. [PubMed: 23093813]

Dietz RR, Davis WL, Harnsberger HR, Jacobs JM, Blatter DD. MR-imaging and MR-angiography in the evaluation of pulsatile tinnitus. American Journal of Neuroradiology. 1994; 15:879–889. [PubMed: 8059655]

Durst CR, Ornan DA, Reardon MA, Mehndiratta P, Mukherjee S, Starke RM, Wintermark M, Evans A, Jensen ME, Crowley RW, Gaughen J, Liu KC. Prevalence of dural venous sinus stenosis and hypoplasia in a generalized population. Journal of Neurointerventional Surgery. 2016 10.1136/neurintsurg-2015-012147.

Dyverfeldt P, Bissell M, Barker AJ, Bolger AF, Carlhall C-J, Ebbers T, Francios CJ, Frydrychowicz A, Geiger J, Giese D, Hope MD, Kilner PJ, Kozerke S, Myerson S, Neubauer S, Wieben O, Markl M. 4D flow cardiovascular magnetic resonance consensus statement. Journal of Cardiovascular Magnetic Resonance. 2015; 17

Eisenman DJ. Sinus wall reconstruction for sigmoid sinus diverticulum and dehiscence: A standardized surgical procedure for a range of radiographic findings. Otology & Neurotology. 2011; 32:1116–1119. [PubMed: 21799456]

Feng W, Utriainen D, Trifan G, Sethi S, Hubbard D, Haacke EM. Quantitative flow measurements in the internal jugular veins of multiple sclerosis patients using magnetic resonance imaging. Reviews on recent clinical trials. 2012; 7:117–126. [PubMed: 22356242]

Gard AP, Klopper HB, Thorell WE. Successful endovascular treatment of pulsatile tinnitus caused by a sigmoid sinus aneurysm a case report and review of the literature. Interventional Neuroradiology. 2009; 15:425–428. [PubMed: 20465881]

Grigioni M, Daniele C, Morbiducci U, Del Gaudio C, D'Avenio G, Balducci A, Barbaro V. A mathematical description of blood spiral flow in vessels: Application to a numerical study of flow in arterial bending. Journal of Biomechanics. 2005; 38:1375–1386. [PubMed: 15922748]

Hofmann E, Behr R, Neumann-Haefelin T, Schwager K. Pulsatile tinnitus: Imaging and differential diagnosis. Deutsches Ärzteblatt International. 2013; 110:451–458. [PubMed: 23885280]

Houdart E, Chapot R, Merland JJ. Aneurysm of a dural sigmoid sinus: A novel vascular cause of pulsatile tinnitus. Annals of Neurology. 2000; 48:669–671. [PubMed: 11026453]

Jayaraman MV, Boxerman JL, Davis LM, Haas RA, Rogg JM. Incidence of extrinsic compression of the internal jugular vein in unselected patients undergoing CT angiography. American Journal of Neuroradiology. 2012; 33:1247–1250. [PubMed: 22322614]

Kefayati S, Holdsworth DW, Poepping TL. Turbulence intensity measurements using particle image velocimetry in diseased carotid artery models: Effect of stenosis severity, plaque eccentricity, and ulceration. Journal of Biomechanics. 2014; 47:253–263. [PubMed: 24182694]

Kefayati S, Kao E, Liu J, Haraldsson H, Faraji F, Ballweber M, Meisel K, Halbach V, Saloner D, Amans M. P-029 Turbulent flow in the venous outflow tract of pulsatile tinnitus patients with sigmoid sinus diverticulum. Journal of Neurointerventional Surgery. 2016; 8:A43.

Khan O, Filippi M, Freedman MS, Barkhof F, Dore-Duffy P, Lassmann H, Trapp B, Bar-Or A, Zak I, Siegel MJ, Lisak R. Chronic cerebrospinal venous insufficiency and multiple sclerosis. Annals of Neurology. 2010; 67:286–290. [PubMed: 20373339]

Krishnan A, Mattox DE, Fountain AJ, Hudgins PA. CT arteriography and venography in pulsatile tinnitus: Preliminary results. American Journal of Neuroradiology. 2006; 27:1635–1638. [PubMed: 16971601]

Madani G, Connor SEJ. Imaging in pulsatile tinnitus. Clinical Radiology. 2009; 64:319–328. [PubMed: 19185662]

Markl M, Schnell S, Barker AJ. 4D flow imaging: Current status to future clinical applications. Current Cardiology Reports. 2014; 16

McTaggart RA, Fischbein NJ, Elkins CJ, Hsiao A, Cutalo MJ, Rosenberg J, Dake MD, Zaharchuk G. Extracranial venous drainage patterns in patients with multiple sclerosis and healthy controls. American Journal of Neuroradiology. 2012; 33:1615–1620. [PubMed: 22517280]

Mehall CJ, Wilner HI, Larouere MJ. Pulsatile tinnitus associated with a laterally placed sigmoid sinus. American Journal of Neuroradiology. 1995; 16:905–907. [PubMed: 7611070]

Okudera T, Huang YP, Ohta T, Yokota A, Nakamura Y, Maehara F, Utsunomiya H, Uemura K, Fukasawa H. Development of posterior-fossa dural sinuses, emissary veins, and jugular bulb - morphological and radiologic study. American Journal of Neuroradiology. 1994; 15:1871–1883. [PubMed: 7863937]

Ong F, Uecker M, Tariq U, Hsiao A, Alley MT, Vasanawala SS, Lustig M. Robust 4D flow denoising using divergence-free wavelet transform. Magnetic Resonance in Medicine. 2015; 73:828–842. [PubMed: 24549830]

Pereira VM, Delattre B, Brina O, Bouillot P, Vargas MI. 4D flow MRI in neuroradiology: Techniques and applications. Topics in magnetic resonance imaging : Topics in Magnetic Resonance Imaging. 2016; 25:81–87. [PubMed: 27049245]

Rayz VL, Boussel L, Acevedo-Bolton G, Martin AJ, Young WL, Lawton MT, Higashida R, Saloner D. Numerical simulations of flow in cerebral aneurysms: Comparison of CFD results and in vivo MRI measurements. Journal of Biomechanical Engineering-Transactions of the ASME130. 2008

Roldan-Alzate A, Francois CJ, Wieben O, Reeder SB. Emerging applications of abdominal 4D flow MRI. AJR. American Journal of Roentgenology. 2016; 207:58–66. [PubMed: 27187681]

Satti SR, Leishangthem L, Chaudry MI. Meta-analysis of CSF diversion procedures and dural venous sinus stenting in the setting of medically refractory idiopathic intracranial hypertension. American Journal of Neuroradiology. 2015; 36:1899–1904. [PubMed: 26251432]

Signorelli F, Mahla K, Turjman F. Endovascular treatment of two concomitant causes of pulsatile tinnitus: Sigmoid sinus stenosis and ipsilateral jugular bulb diverticulum. Case report and literature review. Acta Neurochirurgica. 2012; 154:89–92. [PubMed: 22065197]

Sonmez G, Basekim CC, Ozturk E, Gungor A, Kizilkaya E. Imaging of pulsatile tinnitus: A review of 74 patients. Clinical Imaging. 2007; 31:102–108. [PubMed: 17320776]

Starke RM, Wang T, Ding D, Durst CR, Crowley RW, Chalouhi N, Hasan DM, Dumont AS, Jabbour P, Liu KC. Endovascular treatment of venous sinus stenosis in idiopathic intracranial hypertension: Complications, neurological outcomes, and radiographic results. The Scientific World Journal. 2015; 2015:140408–140408. [PubMed: 26146651]

Stoquart-ElSankari S, Lehmann P, Villette A, Czosnyka M, Meyer ME, Deramond H, Baledent O. A phase-contrast MRI study of physiologic cerebral venous flow. Journal of Cerebral Blood Flow and Metabolism. 2009; 29:1208–1215. [PubMed: 19352399]

Sundstrom P, Wahlin A, Ambarki K, Birgander R, Eklund A, Malm J. Venous and cerebrospinal fluid flow in multiple sclerosis: A case-control study. Annals of Neurology. 2010; 68:255–259. [PubMed: 20695018]

Waldvogel D, Mattle HP, Sturzenegger M, Schroth G. Pulsatile tinnitus - a review of 84 patients. Journal of Neurology. 1998; 245:137–142. [PubMed: 9553842]

Wattjes MP, van Oosten BW, de Graaf WL, Seewann A, Bot JCJ, van den Berg R, Uitdehaag BMJ, Polman CH, Barkhof F. No association of abnormal cranial venous drainage with multiple sclerosis: A magnetic resonance venography and flow-quantification study. Journal of Neurology Neurosurgery and Psychiatry. 2011; 82:429–435.

Weir B. Multiple sclerosis - a vascular etiology? Canadian Journal of Neurological Sciences. 2010; 37:745–757. [PubMed: 21059535]

Weissman JL, Hirsch BE. Imaging of tinnitus: A review. Radiology. 2000; 216:342–349. [PubMed: 10924551]

Zamboni P, Galeotti R, Menegatti E, Malagoni AM, Tacconi G, Dall'Ara S, Bartolomei I, Salvi F. Chronic cerebrospinal venous insufficiency in patients with multiple sclerosis. Journal of Neurology Neurosurgery and Psychiatry. 2009; 80:392–399.

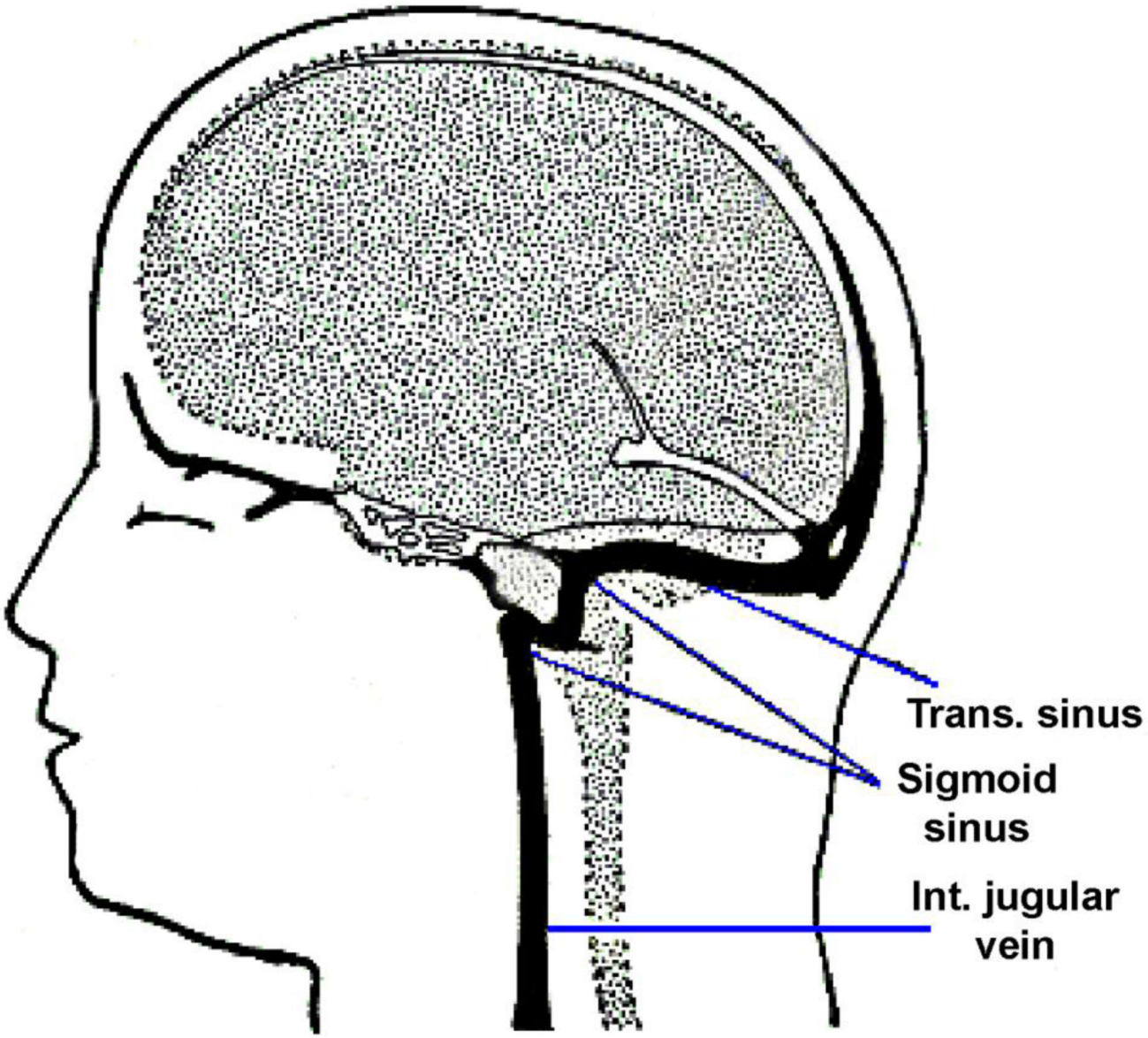

Figure 1.
A schematic of one side of the cerebral venous outflow tract within the human head.

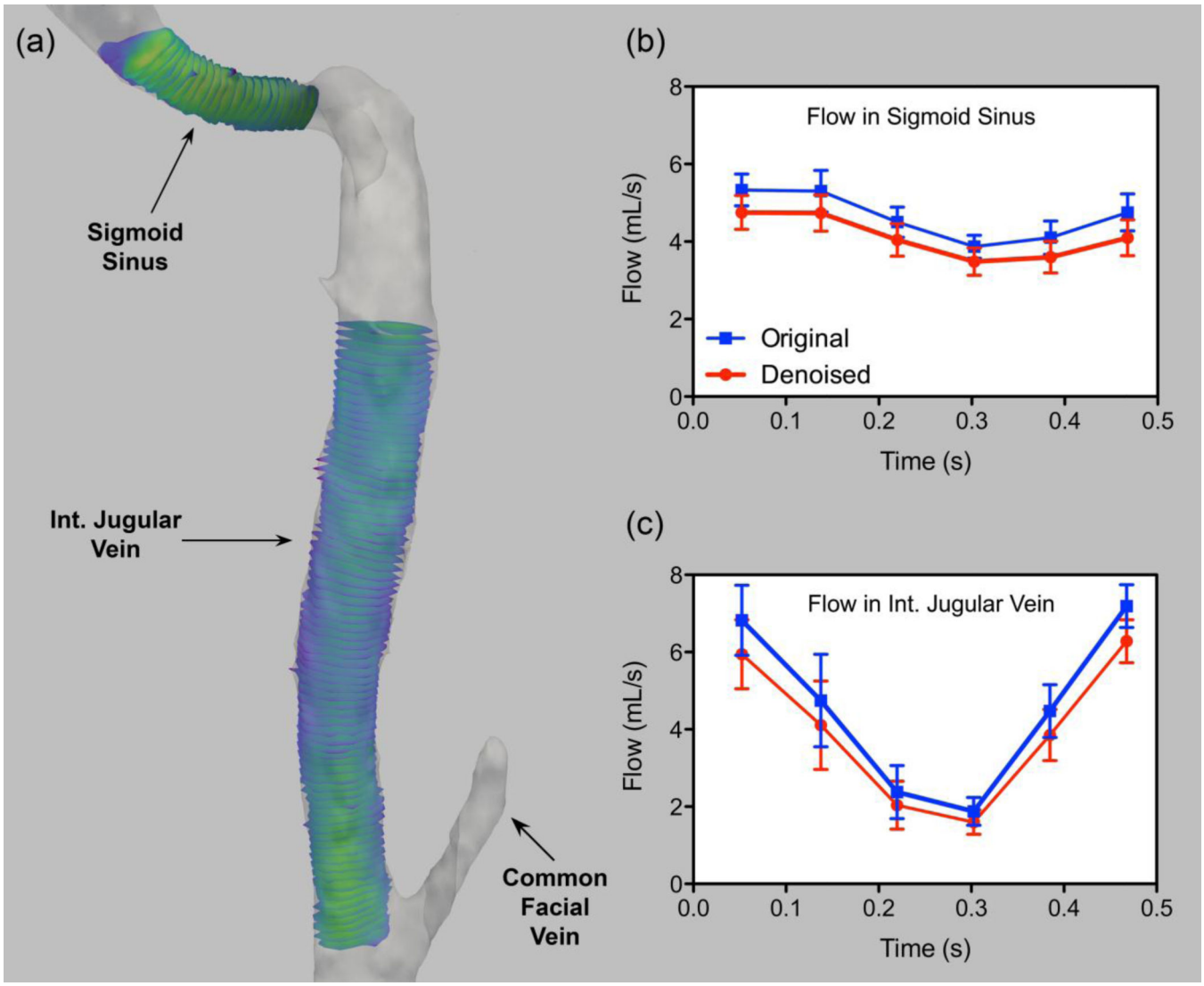

Figure 2.

Flow rate quantification and variation based on the 4D-flow acquisition in a reference jugular vein tract (a) using multiple slices at the sigmoid sinus (b) and downstream of the jugular vein (c). Flow rate estimations are performed on both divergence-free denoised velocity fields and non-filtered ones (original).

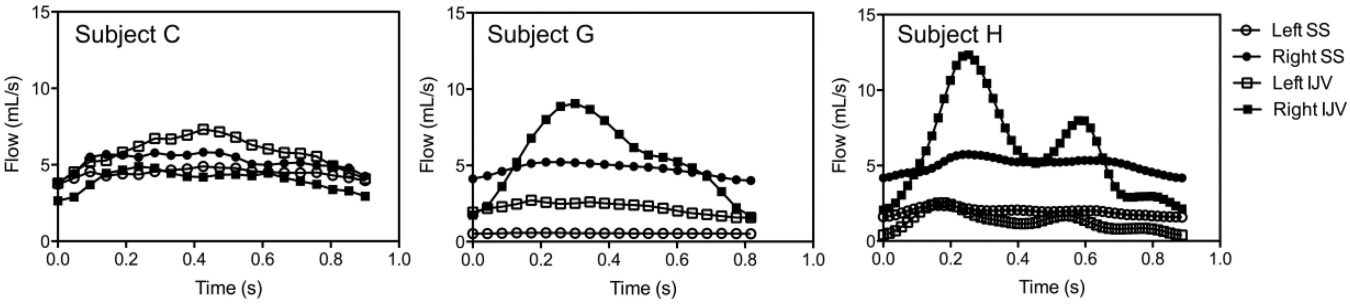

Figure 3.

2D-flow PC-MRI measurements in the sigmoid sinus (SS) and downstream internal jugular vein (IJV) of three subjects for both left (L) and right (R) side venous pathway

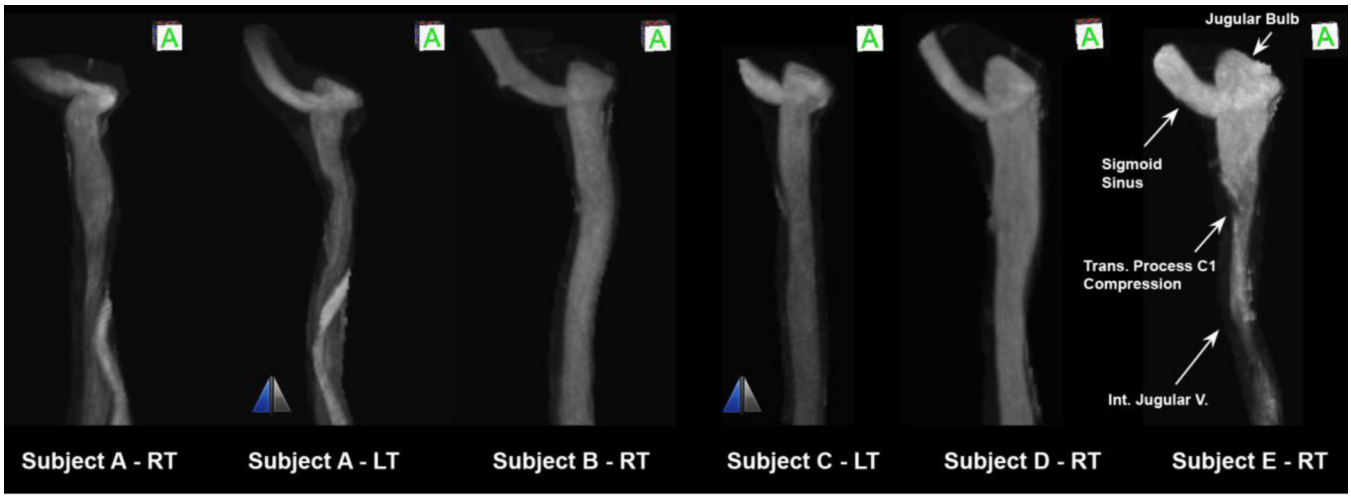

Figure 4.

Anterior view of internal jugular veins of five subjects identified by letters from A to E from combination of right (RT) and left (LT) IJVs sorted from left to right with increasing elevation of jugular bulb from the flooring of the sigmoid sinus junction. The two IJVs with the mirror sign next to them are left-sided IJVs that are mirrored and shown as right-sided IJVs for comparing convenience.

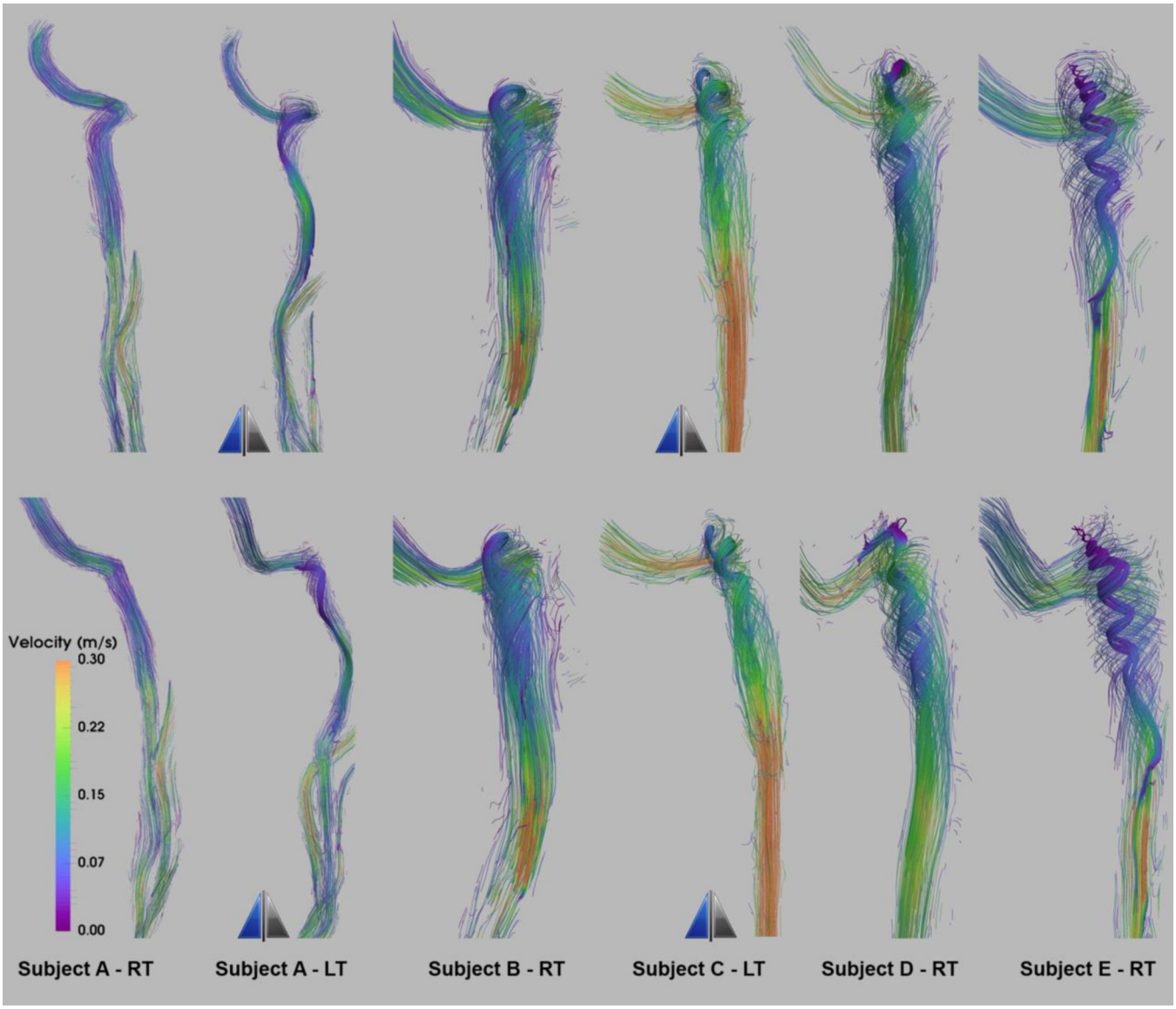

Figure 5.

Velocity streamline visualization of peak-systolic flow in the smooth surface geometries presented in Figure 4. The top panel shows anterior view and bottom panel shows the lateral view. The core flow pattern is highlighted by denser and more intensified streamlines. The two IJVs with the mirror sign next to them are left-sided IJVs, which are mirrored and shown as right-sided IJVs for comparing convenience.

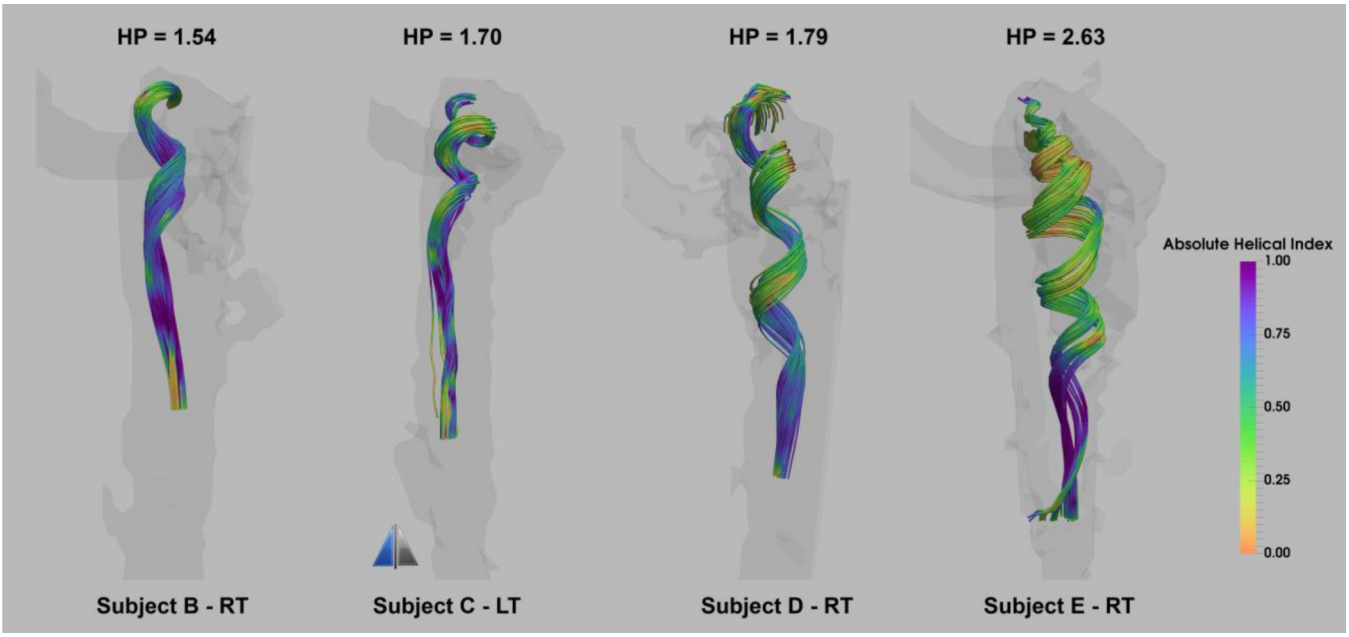

Figure 6.

Core flow visualization of the streamlines colored by absolute helicity index for four of the subjects in the smooth surface group with elevated jugular bulb. The values placed above each geometry are the associated helicity pitch (HP) values. Streamlines are emitted from the focal point of the jugular bulb at peak systole.

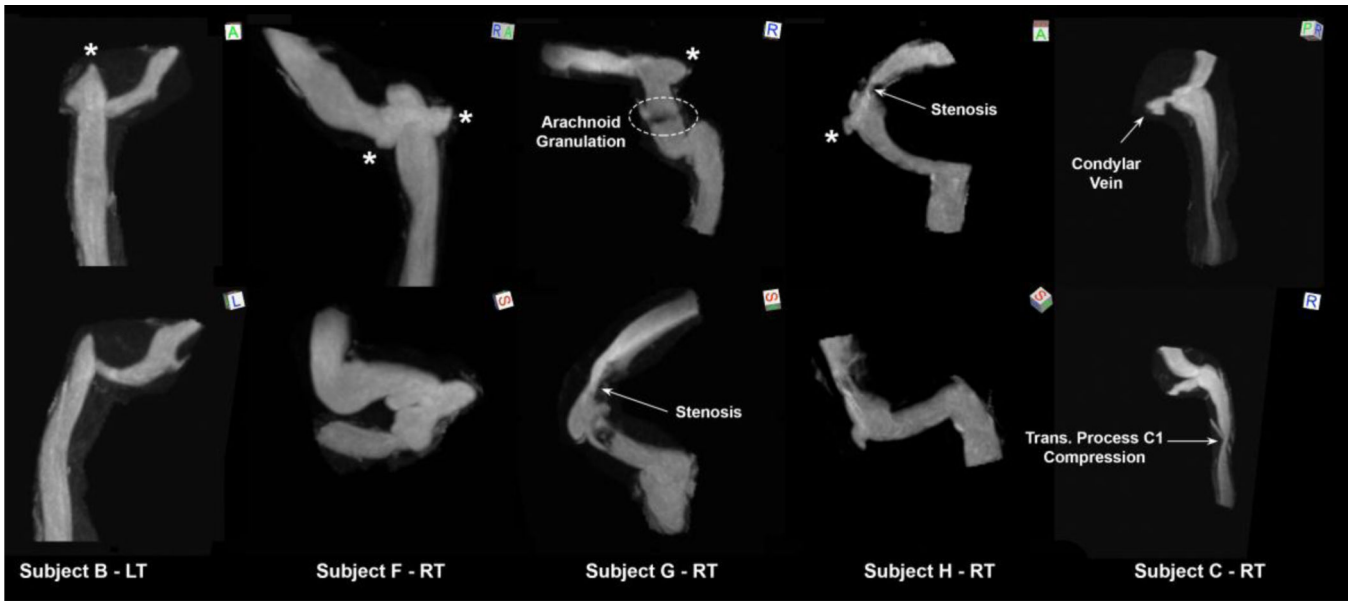

Figure 7.

Series of abnormal venous outflow tracts composing the irregular surface group shown at two different views. The orientation cube references superior (S), inferior (I), anterior (A), posterior (P), left (L), or right (R) view. The asterisk signs next to the geometries mark the diverticula.

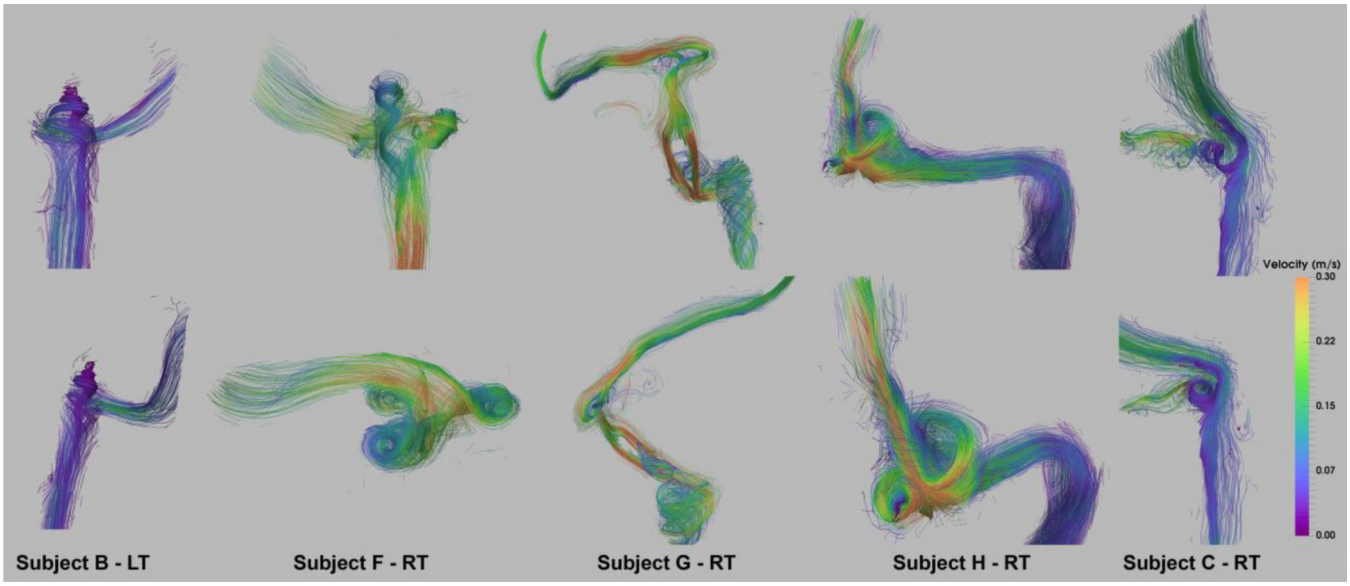

Figure 8.

Velocity streamline visualization of peak-systolic flow in the irregular surface geometries shown in Figure 7 with the matching top and bottom panel views. The main flow pattern is highlighted by denser and more intensified streamlines.

Table 1

Mean flow rate (Q_{mean}) and pulsatility index measured for internal jugular vein (IJV) and sigmoid sinus (SS) for both left (L) and right (R) side of the three subjects shown in Figure 1.

	Mean Flow (mL/s)				Pulsatility Index $[(Q_{max}-Q_{min})/Q_{mean}]$			
	LIJV	**RIJV**	**LSS**	**RSS**	**LIJV**	**RIJV**	**LSS**	**RSS**
Subject C	5.77	3.99	4.44	5.20	0.61	0.56	0.26	0.38
Subject G	2.21	5.41	0.55	4.72	0.52	1.37	0.13	0.26
Subject H	1.30	6.00	1.95	5.04	1.64	1.72	0.40	0.31